DNS OF A SEPARATING TURBULENT BOUNDARY LAYER

Martin Skote and Dan S. Henningson
Department of Mechanics, KTH
S-100 44 Stockholm, Sweden

ABSTRACT

The objective has been to study turbulent boundary layers under adverse pressure gradients (APG) through direct numerical simulation (DNS). The numerical code is based on a pseudo-spectral technique which is suitable for the simple geometry (flat plate) considered here. Five large simulations have been performed, ranging from a zero pressure gradient boundary layer to a separating flow. The simulations have revealed many features of APG turbulent boundary layers which are difficult to capture in experiments. Especially the near-wall behavior has been investigated thoroughly, both through the statistical and instantaneous flow.

Theoretical work based on the turbulent boundary layer equation has been conducted with the aim to develop near-wall laws suitable for turbulence models. The conditions for self-similarity and relations between mean flow parameters have been reviewed and applied in the DNS. The results from the simulations have confirmed the theoretical part of this work.

This paper is based on a recent doctoral thesis (Skote, M., 2001).

INTRODUCTION

The turbulent boundary layer under an APG is decelerated, which does not mean that the turbulence intensity decreases. On the contrary, the flow becomes even more unstable and the turbulence activity is enhanced. The boundary layer also grows (thickens) more rapidly under the influence of an APG. Since the momentum of the fluid is lower close to the wall than further up in the boundary layer, the flow near the wall is more severely affected by the pressure gradient. If the pressure gradient is strong enough, the flow close to the wall separates, i.e. reversed flow appears.

The five simulated cases discussed in this paper are denoted ZPG (zero pressure gradient), A1, A2, A3 (weak, moderate and strong APG), and SEP (separated boundary layer).

GENERAL FEATURES

In figure 1 the freestream velocity (U) for all five simulations are shown. These profiles constitute the boundary condition on the upper edge of the computational box and define the APG. The resulting skin friction ($C_f \equiv 2(u_\tau/U)^2$) of the four attached boundary layers are shown in figure 2. As the APG is increased the C_f is reduced. If the APG is strong enough it induces separation ($C_f < 0$), which occurs for the freestream distribution used in the case SEP. The C_f for SEP is shown in figure 3, where also the C_f distributions for previously completed simulations of a separated turbulent boundary layer are included. The two earlier simulations were performed by Na & Moin (1998) and Spalart & Coleman (1997). In figure 3 the x values have been recalculated in our simulation coordinates. However, the relative starting positions of the boundary layers cannot be calculated and are here matched by letting the starting points of all three simulations be located at $x = 0$. From figure 3 it is clear that the separation bubble is longer in the present simulation (case SEP) than in the other two. In figure 3 the C_f from our simulation has been calculated using the same technique as in Na & Moin (1998) and Spalart & Coleman (1997), i.e. with a value of unity for the freestream velocity.

The streamwise velocity profile at $x = 300$ is shown for the five cases in figure 4. The simulations were performed with different heights of the computational box, as seen in figure 4. The heights in A3 and SEP were actually 65 but the profiles are shown up to 45. The freestream velocity is unity only for ZPG. The profile from SEP exhibits negative values of the velocity close to the wall, showing that separation has occurred.

The streamwise velocity fluctuations form elongated structures near the wall in a ZPG boundary layer. It is generally thought that the structures are weakened in an APG flow. This is illustrated in figure 5, where the streamwise velocity fluctuations in a horizontal plane

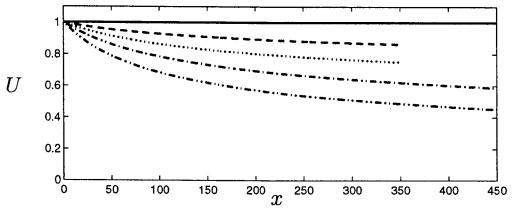

Figure 1: U. — ZPG; - - A1; ··· A2; – · – A3; – · ·– SEP.

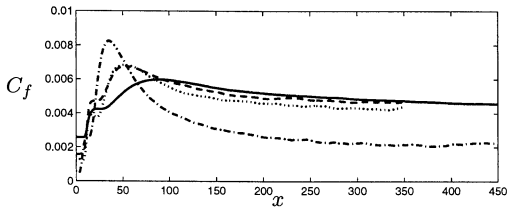

Figure 2: C_f. — ZPG; - - A1; ··· A2; – · – A3.

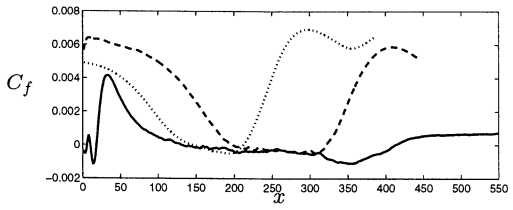

Figure 3: — C_f from SEP; - - C_f from Na & Moin (1998); ··· C_f from Spalart & Coleman (1997).

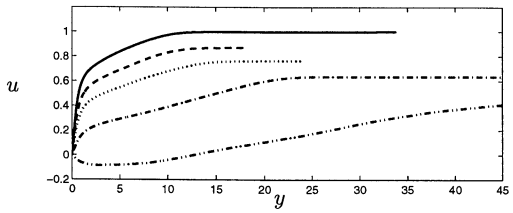

Figure 4: Streamwise velocity profiles at $x = 300$. — ZPG; - - A1; ··· A2; – · – A3; – · ·– SEP.

from ZPG, A3 and SEP are shown. The figure shows the whole computational boxes in the spanwise direction and excluding the transitional part and fringe region in the streamwise direction. The dark color represents the low-speed regions and light color represents the area containing high-speed fluid. The streaks formed in the ZPG case (figure 5a) are spaced 100 viscous units in the spanwise direction. The streaks in the A3 case are shown in figure 5b. The structures are weakened at the end of the domain as compared with those in the beginning, showing the damping effect of the APG on the structures. The spacing between the structures increases from 100 (the same as for a ZPG layer) at the beginning to about 130 at the end, based on the local u_τ.

The SEP case is shown in figure 5c. There are still some structures in the separated flow, though not at all as long and frequent as in the ZPG or A3. Before separation, which occurs at approximately $x = 142$, the streaks are visible, but are rapidly vanishing in the beginning of the separated region. There is notable increase in the streak formation around $x = 350$, where the friction coefficient is at its lowest values, c.f. figure 3. Thus, there are indications that streaks may reappear in a separated region if the back flow is severe enough. After the reattachment at $x = 412$ the streaks are not immediately appearing, but are clearly visible after $x = 450$.

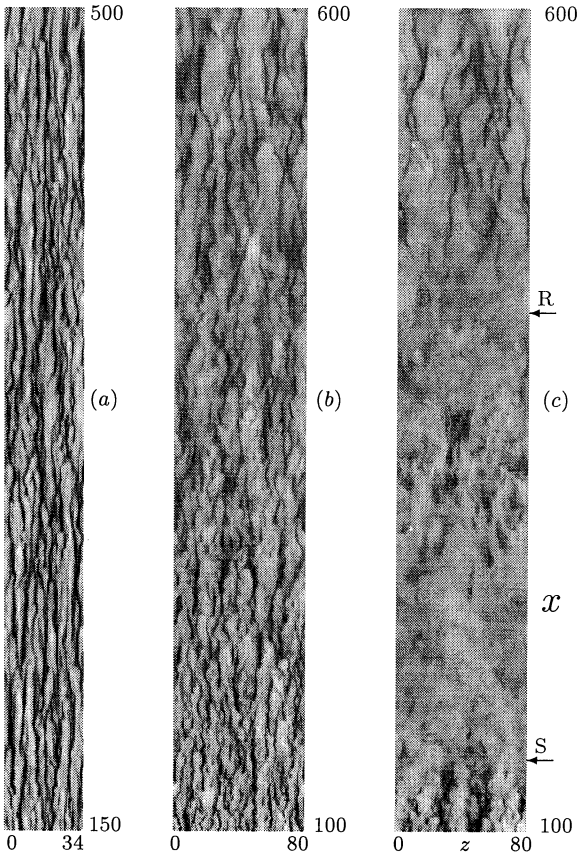

Figure 5: Streamwise velocity fluctuations in a horizontal plane at $y^+ = 10$. (a) ZPG. (b) A3. (c) SEP. The points denoted S and R represent the separation and reattachment respectively.

SCALINGS AND SELF-SIMILARITY

In the outer part of a turbulent boundary layer, the equation of motion can be reduced to,

$$u\frac{\partial u}{\partial x} + v\frac{\partial u}{\partial y} = -\frac{1}{\rho}\frac{dP}{dx} - \frac{\partial}{\partial y}\langle u'v'\rangle. \quad (1)$$

The partial differential equation (1) is converted to an ordinary differential equation through the rescaling,

$$(u-U)/u_\tau = F(\eta), \qquad -\langle u'v'\rangle/{u_\tau}^2 = R(\eta),$$
$$\eta = y/\Delta(x), \qquad \Delta = U\delta^*/u_\tau. \tag{2}$$

U is the freestream velocity, u_τ is the friction velocity and δ^* is the displacement thickness.

The classical treatment of the equations which involves outer and inner equations and a matching of the solutions, leads to the logarithmic friction law,

$$\frac{u_\tau}{U} = \frac{1}{C + \frac{1}{\kappa}\ln Re_{\delta^*}}, \tag{3}$$

where κ is the Kármán constant and $Re_{\delta^*} = U\delta^*/\nu$. Equation (3) shows that $u_\tau/U \to 0$ in the limit of very high Reynolds number.

Letting $u_\tau/U \to 0$, an asymptotic version of equation (1) is obtained.

A different approach to equation (1) is presented in Skote *et al.* (1998), in which the asymptotic theory is substituted with an analysis permitting a finite ratio u_τ/U. Since the logarithmic function grows very slowly when the argument is large, a better assumption than $u_\tau/U \to 0$ for moderately high Reynolds numbers is that $u_\tau/U \approx$ constant. If u_τ/U is regarded as constant and an outer length scale varies linearly, the condition β =constant is fulfilled if the freestream variation is of the form $U \sim x^m$, which was shown by Townsend (1956) and Mellor & Gibson (1966). When specifying a profile in a power-law form it can be written,

$$U = U_0(1 - \frac{x}{x_0})^m. \tag{4}$$

Utilizing these constraints, a non-linear equation is obtained. If now $u_\tau/U \to 0$, the asymptotic version is recovered and is written as,

$$-2\beta F + \frac{\beta}{m}(1+m)\eta\frac{dF}{d\eta} = \frac{dR}{d\eta}. \tag{5}$$

In the inner part of the turbulent boundary layer, the equation of motion can be reduced to,

$$0 = -\frac{1}{\rho}\frac{dP}{dx} + \nu\frac{\partial^2 u}{\partial y^2} - \frac{\partial}{\partial y}\langle u'v'\rangle. \tag{6}$$

Equation (6) can be integrated to give an expression for the total shear stress,

$$\tau^+ = 1 + \left(\frac{u_p}{u_\tau}\right)^3 y^+, \tag{7}$$

with

$$u_p \equiv \left(\nu\frac{1}{\rho}\frac{dP}{dx}\right)^{1/3}. \tag{8}$$

The linear behavior of the total shear stress revealed in equation (7) was first observed by Stratford (1959*a*,*b*).

In the viscous sub-layer the Reynolds shear stress approaches zero and equation (7) can be integrated to give,

$$u^+ = y^+ + \frac{1}{2}\left(\frac{u_p}{u_\tau}\right)^3 (y^+)^2. \tag{9}$$

This equation was first derived by Patel (1973), and reduces to the usual linear profile in ZPG case, when $u_p \to 0$.

The logarithmic expression for the velocity profile in the intermediate layer can be extended for an APG case,

$$u^+ = \frac{1}{\kappa}\left(\ln y^+ - 2\ln\frac{\sqrt{1+\lambda y^+}+1}{2} + 2(\sqrt{1+\lambda y^+}-1)\right) + B, \tag{10}$$

with

$$\lambda = \left(\frac{u_p}{u_\tau}\right)^3.$$

A thorough derivation of equation (10) is given in Skote & Henningson (2001). Townsend (1961) and Mellor (1966) have derived similar equations, albeit with different methods and assumptions.

THE OUTER REGION OF THE BOUNDARY LAYER

Self-similarity

The simulations presented in Skote *et al.* (1998) showed constant β, see table 1. However, the functions $F(\eta)$ and $R(\eta)$ are not self-similar for low Reynolds numbers as shown with DNS in Skote *et al.* (1998). For large Reynolds numbers, the functions $F(\eta)$ and $R(\eta)$ do become self-similar and converge to the asymptotic equation given be equation (5), as shown with turbulence models in Henkes *et al.* (1997) and Henkes (1998).

The shapes of $F(\eta)$ from the simulations are shown in figure 6. The β parameter has a strong influence on the profile shape for A3, while the A1 and A2 profiles are closer to the ZPG profile.

Mean flow parameters

If equation (5) is integrated, the relation

$$m = -\frac{\beta}{1+3\beta} \tag{11}$$

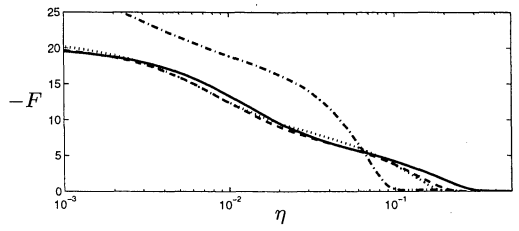

Figure 6: Velocity profiles at $x = 300$. — ZPG; - - A1; ··· A2; – · – A3.

is obtained.

The non-linear equation can also be integrated and yields the relation,

$$m = -\frac{\beta}{H(1+\beta)+2\beta}, \qquad (12)$$

where H is the shape factor. The limit $u_\tau/U \to 0$, can now be obtained by letting $H \to 1$, and the relation (11) is recovered from (12).

To compare the relations (11) and (12), a number of experiments and DNS are summarized in table 1. There is obviously a much better agreement with the non-linear theory, showing that even in high Reynolds number experiments, the asymptotic expressions are of limited value.

The more rapidly U is decreased, the lower C_f is obtained, as shown in figures 1 and 2. While the relative difference in U between the cases remains the same, a dramatic decrease in C_f occurs between A2 and A3. In other words, the closer to separation the boundary layer is, the more sensitive on the freestream velocity distribution it is. The relation between m and β should reveal this behavior. This is seen from figure 7, where equation (12) has been plotted for the two values of H, between which separation has been observed to occur. The limiting value of m increases with H but is confined between -0.22 and -0.25, which is consistent with the observed values in experiments and DNS. The rapid and strongly non-linear approach to separation ($\beta \to \infty$) is consistent with the strong decrease in C_f between A2 and A3 in figure 2.

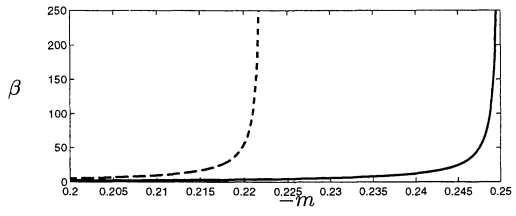

Figure 7: β as a function of m from equation (12) for — H=2.0 and - - H=2.5.

Case	β	H	m	relations (12)	relations (11)
A1	0.24	1.60	-0.077	-0.097	-0.14
A2	0.65	1.63	-0.15	-0.16	-0.22
A3	4.5	1.97	-0.23	-0.23	-0.31
Bradshaw 1	0.9	1.4	-0.15	-0.20	-0.24
Bradshaw 2	5.4	1.54	-0.255	-0.26	-0.31
Skåre & Krogstad	20.0	2.0	-0.22	-0.24	-0.33
Elsberry	25.0	2.45	-0.22	-0.22	-0.33
Stratford	∞	2.5	-0.23	-0.22	-0.33
Spalart & Leonard	1.8	1.65	-0.21	-0.22	-0.28
	8.0	1.92	-0.23	-0.24	-0.32
	∞	2.3	-0.22	-0.23	-0.33
	0.9	1.55	-0.18	-0.19	-0.24
	5.4	1.86	-0.24	-0.24	-0.31

Table 1: Comparison of m from the non-linear/linear theory. The data are taken from the following references (from top to bottom) Skote *et al.* (1998), Skote & Henningson (2001), Bradshaw (1967), Skåre & Krogstad (1994), Elsberry *et al.* (2000), Stratford (1959*a*), Spalart & Leonard (1987).

THE INNER PART OF THE BOUNDARY LAYER

The viscous sub-layer

Profiles in the viscous scaling are compared for the different APG cases in figure 8. All of them matches closely the linear profile $u^+ = y^+$. Thus, even under strong APG the inclusion of the pressure gradient term does not seem to be of importance. However, close to separation or reattachment, when u_τ is small, the velocity profile is strongly influenced by the pressure gradient term. In figure 9, a velocity profile from the SEP case (in the attached region) illustrates the importance of the pressure gradient term.

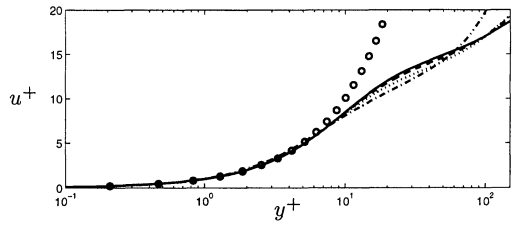

Figure 8: Velocity profiles at $x = 300$. — ZPG; - - A1; ··· A2; – · – A3; ∘ $u^+ = y^+$.

The overlap region

An example of comparison between DNS data and equation (10) is shown in figure 10. DNS data from the attached region (at $x = 450$) of the case SEP is shown as a solid line in figure 10. The dashed line is equation (10) and the dotted line is the logarithmic law for the ZPG boundary layer. The value of additive constant is $B = -2$, which is in agreement with the earlier investigation of the flow just upstream of separation in the simulation of Na &

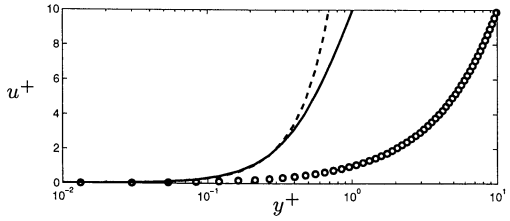

Figure 9: Velocity profile close to reattachment. — SEP; - - equation (9); ∘ $u^+ = y^+$.

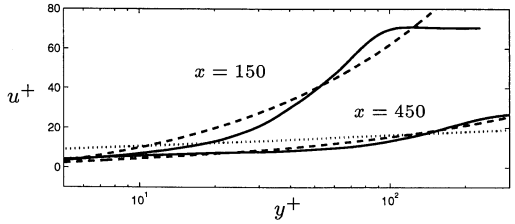

Figure 10: Velocity profiles from SEP: — DNS; - - equation (10) for $x = 450$ and equation (16) for $x = 150$; $\cdots$ $u^+ = \frac{1}{0.41}\ln y^+ + 5.1$.

Moin (1998), see Skote & Henningson (1999).

The value of the Kármán constant, κ, has been set to 0.41 throughout this work. Lately, Österlund *et al.* (2000) have shown that the value of the Kármán constant actually is 0.38 for large enough Reynolds number. However, Spalart (1988) has shown that the old value of 0.41 gives good agreement for low Reynolds numbers. In a number of earlier investigations the influence of the Reynolds number on the Kármán constant has been debated, see e.g. Simpson (1970).

SEPARATION

In Skote & Henningson (2001), one of the boundary layers was separated for a large portion of the flow. The contours of mean streamwise velocity are shown in figure 11 with positive values shown as solid lines and negative as dashed.

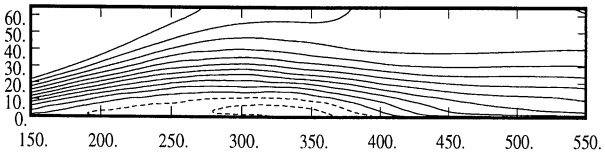

Figure 11: SEP: contours of mean velocity. Positive values shown as solid lines, negative as dashed. Normal direction stretched 20 %.

At the point of separation the wall shear stress is zero, i.e. $u_\tau = 0$. Thus the scaling with u_τ encounters a singularity. When considering a strong APG or separation, the singularity can be avoided by using the velocity scale u_p instead of u_τ. This was noted by Stratford (1959*b*), Townsend (1961) and Tennekes & Lumley (1972). By rescaling equation (9) the

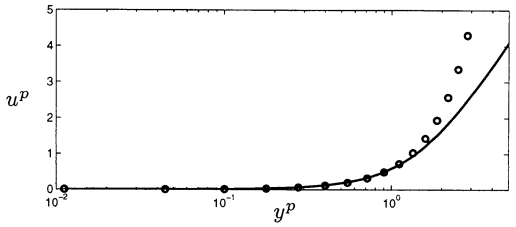

Figure 12: Velocity profile close to reattachment. — SEP; ∘ $u^p = \frac{1}{2}(y^p)^2$.

following expression for the velocity profile in the viscous sub-layer is obtained,

$$u^p \equiv \frac{u}{u_p} = \frac{1}{2}(y^p)^2 + \left(\frac{u_\tau}{u_p}\right)^2 y^p, \qquad (13)$$

where $y^p \equiv y u_p/\nu$. In the limit of separation, when $u_\tau \to 0$, equation (13) reduces to

$$u^p = \frac{1}{2}(y^p)^2. \qquad (14)$$

Thus, in this rescaled form, the singularity is avoided. The profile from the SEP case at reattachment is shown in figure 12 together with the asymptotic expression (14). This is the same velocity profile as was shown in figure 9. Equation (10) can be rewritten in the pressure gradient scaling for the overlap region, and the resulting expression asymptotes to the square-root law when $u_\tau \to 0$,

$$u^p = \frac{1}{\kappa} 2\sqrt{y^p} + C, \qquad (15)$$

which was first obtained by Stratford (1959*b*).

The velocity profile in the overlap region becomes, in the separated region,

$$u^+ = \frac{1}{\kappa}\left[2\sqrt{\lambda y^+ - 1} - 2\arctan\left(\sqrt{\lambda y^+ - 1}\right)\right] + B. \qquad (16)$$

One of the profiles (at $x = 150$) from the separated region is shown in figure 10 together with the profile given by equation (16). The additive constant is $B = -7$ for the separated case. Observe that no part of the back-flow region is shown in figure 10. The reader is referred to Skote & Henningson (2001) for velocity profiles in the back-flow region.

REFERENCES

BRADSHAW, P. 1967 The turbulent structure of equilibrium boundary layers. *J. Fluid Mech.* **29**, 625–645.

ELSBERRY, K., LOEFFLER, J., ZHOU, M. D. & WYGNANSKI, I. 2000 An experimental study of a boundary layer that is maintained on the verge of separation. *J. Fluid Mech.* **423**, 227–261.

HENKES, R. A. W. M. 1998 Scaling of equilibrium boundary layers under adverse pressure gradient using turbulence models. *AIAA J.* **36**, 320–326.

HENKES, R. A. W. M., SKOTE, M. & HENNINGSON, D. S. 1997 Application of turbulence models to equilibrium boundary layers under adverse pressure gradient. Eleventh Symposium on Turbulent Shear Flows, Grenoble, France.

MELLOR, G. L. 1966 The effects of pressure gradients on turbulent flow near a smooth wall. *J. Fluid Mech.* **24**, 255–274.

MELLOR, G. L. & GIBSON, D. M. 1966 Equilibrium turbulent boundary layers. *J. Fluid Mech.* **24**, 225–253.

NA, Y. & MOIN, P. 1998 Direct numerical simulation of a separated turbulent boundary layer. *J. Fluid Mech.* **374**, 379–405.

ÖSTERLUND, J. M., JOHANSSON, A. V., NAGIB, H. M. & HITES, M. H. 2000 A note on the overlap region in turbulent boundary layers. *Phys. Fluids* **12**, 1–4.

PATEL, V. C. 1973 A unified view of the law of the wall using mixing-length theory. *Aeronaut. Q.* **24**, 55–70.

SIMPSON, R. L. 1970 Characteristics of turbulent boundary layers at low Reynolds numbers with and without transpiration. *J. Fluid Mech.* **42**, 769–802.

SKÅRE, P. E. & KROGSTAD, P.-Å. 1994 A turbulent equilibrium boundary layer near separation. *J. Fluid Mech.* **272**, 319–348.

SKOTE, M., HENKES, R. A. W. M. & HENNINGSON, D. S. 1998 Direct numerical simulation of self-similar turbulent boundary layers in adverse pressure gradients. *Flow, Turbulence and Combustion* **60**, 47–85.

SKOTE, M. & HENNINGSON, D. 1999 Analysis of the data base from a DNS of a separating turbulent boundary layer. Center for Turbulence Research, Annual Research Briefs 1999, 225–237.

SKOTE, M. & HENNINGSON, D. S. 2001 Direct numerical simulation of a separating turbulent boundary layer. *J. Fluid Mech.* (Submitted).

SKOTE, M. 2001 Studies of turbulent boundary layer flow through direct numerical simulation. PhD thesis, Royal Institute of Technology, Stockholm, Sweden.

SPALART, P. R. 1988 Direct simulation of a turbulent boundary layer up to $Re_\theta = 1410$. *J. Fluid Mech.* **187**, 61–98.

SPALART, P. R. & COLEMAN, G. N. 1997 Numerical study of a separation bubble with heat transfer. *European J. Mechanics B/Fluids* **16**, 169.

SPALART, P. R. & LEONARD, A. 1987 Direct numerical simulation of equilibrium turbulent boundary layers. In *Turbulent Shear Flows 5* (eds. F. Durst, B. E. Launder, J. L. Lumley, F. W. Schmitd & J. H. Whitelaw), pp. 234–252. Springer-Verlag.

STRATFORD, B. S. 1959*a* An experimental flow with zero skin friction throughout its region of pressure rise. *J. Fluid Mech.* **5**, 17–35.

STRATFORD, B. S. 1959*b* The prediction of separation of the turbulent boundary layer. *J. Fluid Mech.* **5**, 1–16.

TENNEKES, H. & LUMLEY, J. L. 1972 *A First Course in Turbulence*. The MIT Press.

TOWNSEND, A. A. 1956 *The structure of turbulent shear flow*. Cambridge University Press.

TOWNSEND, A. A. 1961 Equilibrium layers and wall turbulence. *J. Fluid Mech.* **11**, 97–120.